Zinc diffusion in gallium arsenide and the properties of gallium interstitials

H. Bracht* and S. Brotzmann
Institute of Materials Physics, University of Münster, D-48149 Münster, Germany
(Received 3 November 2004; published 31 March 2005)

We have performed zinc diffusion experiments in gallium arsenide at temperatures between 620 °C and 870 °C with a dilute Ga-Zn source. The low Zn partial pressure established during annealing realizes Zn surface concentrations of $\leqslant 2\times10^{19}$ cm^{-3}, which lead to the formation of characteristic S-shaped diffusion profiles. Accurate modeling of the Zn profiles, which were measured by means of secondary ion mass spectroscopy, shows that Zn diffusion under the particular doping conditions is mainly mediated by neutral and singly positively charged Ga interstitials via the kick-out mechanism. We determined the temperature dependence of the individual contributions of neutral and positively charged Ga interstitials to Ga diffusion for electronically intrinsic conditions. The data are lower than the total Ga self-diffusion coefficient and hence consistent with the general interpretation that Ga diffusion under intrinsic conditions is mainly mediated by Ga vacancies. Our results disprove the general accepted interpretation of Zn diffusion in GaAs via doubly and triply positively charged Ga interstitials and solves the inconsistency related to the electrical compensation of the acceptor dopant Zn by the multiply charged Ga interstitials.

DOI: 10.1103/PhysRevB.71.115216 PACS number(s): 61.72.Ji, 66.30.Dn, 66.30.Hs, 66.30.Jt

I. INTRODUCTION

Zinc (Zn) is one of the most commonly used impurities for *p*-type doping of GaAs and AlGaAs because of its high solubility, fast diffusion and low ionization energy. The diffusion of Zn in GaAs has been studied extensively in the last 30 years as documented by the numerous papers published on Zn diffusion and its simulation.[1–13] According to Gösele and Morehead[5] and more recent results of Yu *et al.*[12] and Bösker *et al.*,[13] Zn diffusion in GaAs is generally considered to proceed via the kick-out mechanism

$$\mathrm{Zn}_i^+ \rightleftharpoons \mathrm{Zn}_{\mathrm{Ga}}^- + I_{\mathrm{Ga}}^{2+}. \tag{1}$$

Zn_i, $\mathrm{Zn}_{\mathrm{Ga}}$, and I_{Ga} denote the interstitially and substitutionally dissolved Zn and a Ga interstitial, respectively. The superscripts indicate the charge state of the particular point defect. In addition to the participation of I_{Ga}^{2+}, a contribution of I_{Ga}^{3+} was proposed by Bösker *et al.*[13] in order to describe two step Zn diffusion profiles. Similar kink-and-tail profiles are known to develop in the very high concentration region ($C_{\mathrm{Zn}} \gtrsim 10^{20}$ cm^{-3}). These profiles are associated with the formation of voids and interstitial-type dislocation loops.[1,12,14,15] However, kink-and-tail profiles were also observed in samples which contain no voids or dislocation loops.[13] These profiles given by Bösker *et al.*[13] were analyzed on the basis of the kick-out mechanism assuming $I_{\mathrm{Ga}}^{2+,3+}$. A major drawback of the diffusion model is that the high equilibrium concentration of I_{Ga}^{2+}, which is required to reproduce the tail of the acceptor dopant profiles, leads to almost complete electrical compensation of the acceptors near the diffusion front.[13] Had the authors considered compensation, the calculated $\mathrm{Zn}_{\mathrm{Ga}}$ profile would be not as steep at the diffusion front as the experimental profile.

Recently one of us (H.B.) investigated Zn-enhanced Ga diffusion in GaAs isotope multilayer structures[17] in order to study impurity-induced layer disordering (IILD) in group III-V compound semiconductors which was discovered by Laidig *et al.*[18] The Zn and Ga diffusion profiles, which were simultaneously recorded by means of secondary ion mass spectrometry (SIMS), as well as earlier Zn and Cd diffusion profiles, were accurately described by the following set of defect reactions:[17]

$$A_i^+ \rightleftharpoons A_{\mathrm{Ga}}^- + I_{\mathrm{Ga}}^0 + 2h, \tag{2}$$

$$A_i^+ + V_{\mathrm{Ga}}^0 \rightleftharpoons A_{\mathrm{Ga}}^- + 2h, \tag{3}$$

$$A_i^+ + V_{\mathrm{Ga}}^+ \rightleftharpoons A_{\mathrm{Ga}}^- + 3h. \tag{4}$$

Here A represents the acceptor dopant Zn or Cd. V_{Ga}^0, V_{Ga}^+, I_{Ga}^0, and h denote neutral and singly positively charged Ga vacancies, neutral Ga self-interstitials, and holes, respectively. On the basis of reactions (2)–(4) the kink-and-tail dopant profiles and, simultaneously, the interdiffusion of the ^{69}GaAs/^{71}GaAs layers were reproduced. In addition, kink-and-tail Zn and Cd profiles from the literature[13,16] were described.[17] On the basis of reactions (2)–(4) the near-surface kink is a consequence of V_{Ga}^0- and V_{Ga}^+-controlled dopant diffusion. The profile tail is shaped by the diffusion of I_{Ga}^0, and the maximum penetration depth is related to the diffusion of A_i.

In order to investigate the validity of reactions (2)–(4) and, in particular, to determine the charge states of the Ga interstitials we performed additional Zn diffusion experiments. The experiments were carried out under conditions that suppress the formation of the near-surface kink. The observed characteristic S-shaped Zn profiles provide strong evidence of an I_{Ga}^0- and I_{Ga}^+-mediated Zn diffusion.

II. EXPERIMENT

Samples with typical lateral dimensions of 6 mm $\times$ 10 mm were cut from a semi-insulating GaAs wafer with a thickness of 500 μm. The samples were rinsed in organic

solvents, etched in dilute HCl, and purged with deionized water. Then they were sealed in evacuated silica ampoules together with about 50 mg of a Ga-Zn alloy. Alloys with less than 1.0 at.% Zn were used as diffusion source in order to significantly reduce the Zn partial pressure during annealing. In this way a concentration of substitutional Zn at the surface of about 10^{19} cm^{-3} is established. The diffusion anneals were performed in a resistance-heated furnace at temperatures between 620 °C and 870 °C for times that are appropriate to realize penetration depths of less than 5 μm. The temperature was controlled with an accuracy of ±2 K. The diffusion process was terminated by rapidly cooling the ampoule with ethylene glycol down to room temperature.

Zn profiles were measured by means of electrochemical capacitance voltage (ECV) profiling (BioRad PN4400 system) and secondary ion mass spectrometry (SIMS) using a Cs^+ ion-beam with an energy of 10 keV. SIMS analyses were performed on a CAMECA IMS-4f at the Institute of Fresenius (Dresden, Germany). The depths of the craters left from the ECV and SIMS analyses were determined with a surface profilometer with an accuracy of about 5%. The measured secondary ion counts were converted into concentrations, taking into account a homogeneously doped GaAs wafer with a Zn concentration of 3.0×10^{18} cm^{-3} as reference sample. The free hole concentration of this reference sample was checked with ECV profiling. Since Zn in GaAs is a shallow acceptor and mainly dissolved on the substitutional Ga sites, the measured hole concentration equals to a good approximation the total Zn concentration.

The shape of the Zn profiles recorded by ECV profiling can be affected by nonuniform etching of the crater, which is typically 3 mm in diameter, and by contributions of the crater shell to the measured capacitance. SIMS measurements were typically performed on a flat 175 μm$\times$175 μm area whereby secondary ions were only collected from an inner area of 50 μm in diameter. In this way instrumental broadening effects due to secondary ions released from the crater edges were reduced. Taking into account the peculiarities of the respective ECV and SIMS profiling methods, SIMS measurements are considered to provide a better representation of the actual Zn profile than ECV measurements. Accordingly, only the profiles measured with SIMS were taken into account for detailed modeling.

In order to select appropriate Zn-diffused GaAs samples for SIMS analyses all samples were first investigated with ECV profiling. Hole concentration profiles with a kink-and-tail shape were observed after diffusion annealing in the case when a Ga-Zn source with 1 at.% Zn was used. Further reduction of the Zn content in the alloy was achieved by multiple use of the same Ga-Zn source. With continuing depletion of the source the Zn boundary concentration also decreases. The impact of the source depletion on the shape of the Zn profile is illustrated in Fig. 1. Although we cannot specify the actual amount of Zn in the source after its multiple use, Fig. 1 clearly demonstrates that the shape of the profile changes from a kink-and-tail to a S-shaped profile.

Samples with S-shaped profiles identified by ECV profiling were subsequently analyzed with SIMS to determine the shape of the profile more accurately. Figures 2 and 3 show SIMS concentration profiles measured after diffusion annealing at temperatures between 620 °C and 870 °C. All profiles clearly exhibit a S-shaped form. The upper profile in Fig. 3 shows the hole concentration profile, which was measured with ECV profiling after diffusion at 820 °C for 1 h. A comparison with the corresponding SIMS profile shows that the shape of the ECV and SIMS profiles are qualitatively similar. Up to a depth of ~1 μm the hole and total Zn concentration are equal within the accuracy of both methods. However, the

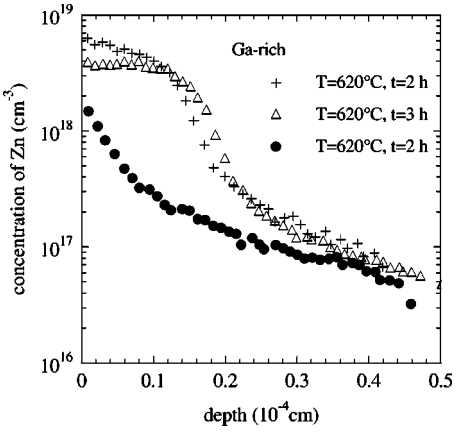

FIG. 1. Hole concentration profiles of Zn-diffused GaAs samples measured by means of ECV profiling. Diffusion anneals were performed with a dilute Ga-Zn source at temperatures and times as indicated. Multiple use of the Ga-Zn alloy reduces the amount of Zn and therewith the Zn-partial pressure established during annealing. As a consequence the hole concentration at the surface decreases. Along with the reduction of the boundary concentration the profiles indicate a change from a kink-and-tail shape to a S-shaped form. For clarity only every second data point is shown.

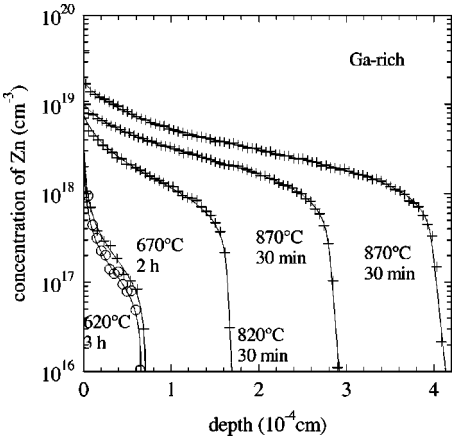

FIG. 2. Concentration profiles of Zn measured with SIMS after diffusion at temperatures and times as indicated. The solid lines are best fits to the experimental profiles that were obtained on the basis of the kick-out reaction (5) taking into account I^0_{Ga} and I^+_{Ga}. Note, the different penetration depths of the two uppermost Zn profiles, which both were obtained after diffusion annealing at 870 °C for 30 min, reflect the doping dependence of the Zn diffusion coefficient $D^{eff}_{Zn_{Ga}^-}$ (see Sec. IV A). According to this doping dependence the profile with the higher Zn surface concentration is expected to exhibit a higher penetration depth. For clarity only every tenth experimental data point is shown.

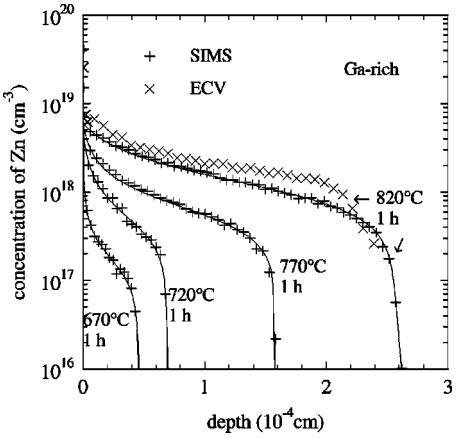

FIG. 3. Concentration profiles of Zn measured with SIMS after diffusion at temperatures and times as indicated. The solid lines are best fits to the experimental profiles that were obtained on the basis of the kick-out reaction (5), taking into account I^0_{Ga} and I^+_{Ga}. For clarity only every tenth SIMS data point is shown. The upper curve (×) shows the hole concentration profile of the sample annealed at 820 °C which was measured by means of ECV profiling (only every third data point is shown).

shape of the ECV profile in the range of 1 to 2.5 μm deviates from the SIMS measurement. This deviation is attributed to instrumental broadening effects related to ECV profiling (see above), which are considered to be more severe than the instrumental broadening due to SIMS profiling. Therefore, only the SIMS measurements were taken into account for a detailed analysis of the Zn profiles.

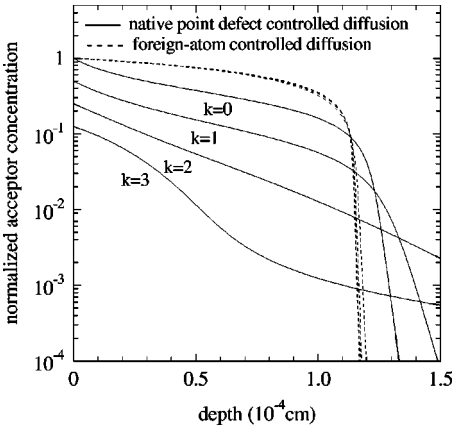

FIG. 4. Normalized concentration profiles of an acceptor dopant *A* calculated on the basis of the kick-out reaction (5) for various charge states *k* of I^k_{Ga}. Solid (dashed) lines represent diffusion profiles, which are expected in the case of the native point defect (foreign-atom) controlled diffusion mode. The calculations demonstrate that the shape of the dopant profile depends on the charge state of I^k_{Ga} only in the case when the diffusion of the dopant is controlled by the native point defect. For the foreign-atom-controlled mode all charge states of I^k_{Ga} predict similar box-shaped profiles. For a better representation of the profile shape near the surface (depth $\leqslant 0.5$ μm) the profiles calculated for the I^{3+}_{Ga}-, I^{2+}_{Ga}-, and I^+_{Ga}-mediated dopant diffusion were divided by 8, 4, and 2, respectively.

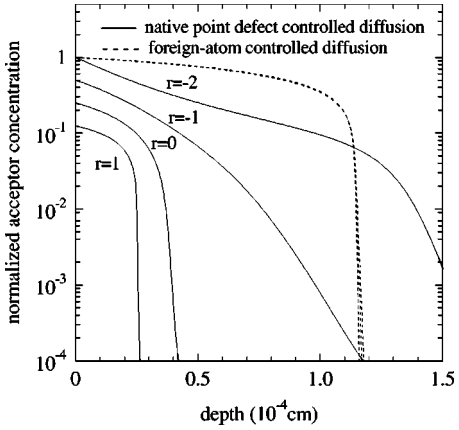

FIG. 5. Normalized concentration profiles of an acceptor dopant *A* calculated on the basis of the dissociative mechanism (6) for various charge states *r* of V^r_{Ga}. Solid (dashed) lines represent diffusion profiles, which are expected in the case of the native point defect- (foreign-atom) controlled diffusion mode. The calculations demonstrate that the shape of the dopant profile depends on the charge state of V^r_{Ga} only in the case when the diffusion of the dopant is controlled by the native point defect. For the foreign-atom-controlled mode all charge states of V^r_{Ga} predict similar box-shaped profiles. For a better representation of the profile shape near the surface (depth $\leqslant 0.5$ μm) the profiles calculated for the V^+_{Ga}-, V^0_{Ga}-, and V^-_{Ga}-mediated dopant diffusion were divided by 8, 4, and 2, respectively.

III. ANALYSIS

For modeling Zn diffusion we consider both the kick-out mechanism

$$Zn_i^+ \rightleftharpoons Zn_{Ga}^- + I^k_{Ga} + (2-k)h \tag{5}$$

and the dissociative mechanism

$$Zn_i^+ + V^r_{Ga} \rightleftharpoons Zn_{Ga}^- + (2+r)h. \tag{6}$$

k and *r* in reactions (5) and (6) represent the charge states of I^k_{Ga} and V^r_{Ga}, respectively. Figure 4 illustrates diffusion profiles that are expected in the case when Zn diffuses via reaction (5). Two different diffusion modes are distinguished. These are the native point defect- and foreign-atom-controlled modes. In the former mode the supply of Zn_i from the surface is faster than the removal of I_{Ga} created by the $Zn_i \rightarrow Zn_{Ga}$ exchange. This mode predicts profiles which are specific with respect to the charge state *k* of I^k_{Ga} (see solid lines in Fig. 4). In the latter mode the supply of Zn_i determines the formation of Zn_{Ga}. In this case the dopant profile is independent of the charge state of I^k_{Ga} (see dashed lines in Fig. 4). Similar calculations were performed on the basis of the dissociative mechanism (6). The results are shown by the lines in Fig. 5. In the case of the native defect-controlled diffusion mode the calculated profiles (see solid lines) reveal a strong dependence on the charge state *r* of V^r_{Ga}. For the foreign-atom-controlled mode the calculated profiles are independent of V^r_{Ga} (see dashed lines in Fig. 5). Note, the kick-out and dissociative mechanisms predict the same box-shaped dopant profiles in the foreign-atom-controlled mode.

Profiles that belong to this mode cannot aid in distinguishing between the kick-out and dissociative mechanisms.

A qualitative comparison of the profiles shown in Figs. 2 and 3 with the simulations illustrated in Figs. 4 and 5 indicates that the native defect-controlled diffusion mode predicts dopant diffusion profiles that are very similar to the experiment. More specifically, the I_{Ga}^{0}- and I_{Ga}^{+}-controlled diffusion via reaction (5) and the V_{Ga}^{2-}-controlled diffusion via reaction (6) predict S-shaped dopant profiles. However, a contribution of V_{Ga}^{2-} is very unlikely because acceptor doping is expected to suppress the formation of negatively charged defects. Moreover, our experiments were performed under Ga-rich conditions, which favors the formation of I_{Ga} and suppresses the formation of V_{Ga}. Hence the diffusion profiles shown in Figs. 2 and 3 are considered to be a consequence of the kick-out reaction (5), which involves I_{Ga}^{0} and I_{Ga}^{+}.

A. Modeling of Zn diffusion

The mathematical formulation of Zn diffusion on the basis of reaction (5) with I_{Ga}^{0} and I_{Ga}^{+} is given by the following set of four coupled partial differential equations

$$\frac{\partial \tilde{C}_{\mathrm{Zn}_{\mathrm{Ga}}^{-}}}{\partial t} = k_b' C_{I_{\mathrm{Ga}}^{0}}^{\mathrm{eq}} (p^{\mathrm{eq}})^2 (\tilde{C}_{\mathrm{Zn}_i^{+}} - \tilde{C}_{\mathrm{Zn}_{\mathrm{Ga}}^{-}} \tilde{C}_{I_{\mathrm{Ga}}^{0}} \tilde{p}^2) + k_b'' C_{I_{\mathrm{Ga}}^{+}}^{\mathrm{eq}} p^{\mathrm{eq}} (\tilde{C}_{\mathrm{Zn}_i^{+}} - \tilde{C}_{\mathrm{Zn}_{\mathrm{Ga}}^{-}} \tilde{C}_{I_{\mathrm{Ga}}^{+}} \tilde{p}), \tag{7}$$

$$\frac{C_{\mathrm{Zn}_i^{+}}^{\mathrm{eq}}}{C_{\mathrm{Zn}_{\mathrm{Ga}}^{-}}^{\mathrm{eq}}} \frac{\partial \tilde{C}_{\mathrm{Zn}_i^{+}}}{\partial t} = \frac{C_{\mathrm{Zn}_i^{+}}^{\mathrm{eq}} D_{\mathrm{Zn}_i^{+}}}{C_{\mathrm{Zn}_{\mathrm{Ga}}^{-}}^{\mathrm{eq}}} \frac{\partial}{\partial x} \left(\frac{\partial \tilde{C}_{\mathrm{Zn}_i^{+}}}{\partial x} - \frac{\tilde{C}_{\mathrm{Zn}_i^{+}}}{p} \frac{\partial p}{\partial x} \right) - \frac{\partial \tilde{C}_{\mathrm{Zn}_{\mathrm{Ga}}^{-}}}{\partial t}, \tag{8}$$

$$\frac{C_{I_{\mathrm{Ga}}^{0}}^{\mathrm{eq}}}{C_{\mathrm{Zn}_{\mathrm{Ga}}^{-}}^{\mathrm{eq}}} \frac{\partial \tilde{C}_{I_{\mathrm{Ga}}^{0}}}{\partial t} = \frac{C_{I_{\mathrm{Ga}}^{0}}^{\mathrm{eq}} D_{I_{\mathrm{Ga}}^{0}}}{C_{\mathrm{Zn}_{\mathrm{Ga}}^{-}}^{\mathrm{eq}}} \frac{\partial^2 \tilde{C}_{I_{\mathrm{Ga}}^{0}}}{\partial x^2} + k_b' C_{I_{\mathrm{Ga}}^{0}}^{\mathrm{eq}} (p^{\mathrm{eq}})^2 (\tilde{C}_{\mathrm{Zn}_i^{+}} - \tilde{C}_{\mathrm{Zn}_{\mathrm{Ga}}^{-}} \tilde{C}_{I_{\mathrm{Ga}}^{0}} \tilde{p}^2), \tag{9}$$

$$\frac{C_{I_{\mathrm{Ga}}^{+}}^{\mathrm{eq}}}{C_{\mathrm{Zn}_{\mathrm{Ga}}^{-}}^{\mathrm{eq}}} \frac{\partial \tilde{C}_{I_{\mathrm{Ga}}^{+}}}{\partial t} = \frac{C_{I_{\mathrm{Ga}}^{+}}^{\mathrm{eq}} D_{I_{\mathrm{Ga}}^{+}}}{C_{\mathrm{Zn}_{\mathrm{Ga}}^{-}}^{\mathrm{eq}}} \frac{\partial}{\partial x} \left(\frac{\partial \tilde{C}_{I_{\mathrm{Ga}}^{+}}}{\partial x} - \frac{\tilde{C}_{I_{\mathrm{Ga}}^{+}}}{p} \frac{\partial p}{\partial x} \right) + k_b'' C_{I_{\mathrm{Ga}}^{+}}^{\mathrm{eq}} p^{\mathrm{eq}} (\tilde{C}_{\mathrm{Zn}_i^{+}} - \tilde{C}_{\mathrm{Zn}_{\mathrm{Ga}}^{-}} \tilde{C}_{I_{\mathrm{Ga}}^{+}} \tilde{p}). \tag{10}$$

$\tilde{C}_X$ and D_X with $X \in \{\mathrm{Zn}_{\mathrm{Ga}}^{-}, \mathrm{Zn}_i^{+}, I_{\mathrm{Ga}}^{0,+}\}$ are the normalized concentrations $\tilde{C}_X = C_X / C_X^{\mathrm{eq}}$ and diffusion coefficients of the particular point defect, respectively. $\tilde{p}$ represents the normalized hole concentration $\tilde{p} = p/p^{\mathrm{eq}}$. k_b' and k_b'' denote the backward rate constants of reaction (5) for $k=0$ and $k=1$, respectively. Applying the law of mass action to reaction (5), the forward rate constants k_f were substituted by

$$k_f' = k_b' \frac{C_{\mathrm{Zn}_{\mathrm{Ga}}^{-}}^{\mathrm{eq}} C_{I_{\mathrm{Ga}}^{0}}^{\mathrm{eq}} (p^{\mathrm{eq}})^2}{C_{\mathrm{Zn}_i^{+}}^{\mathrm{eq}}}, \tag{11}$$

$$k_f'' = k_b'' \frac{C_{\mathrm{Zn}_{\mathrm{Ga}}^{-}}^{\mathrm{eq}} C_{I_{\mathrm{Ga}}^{+}}^{\mathrm{eq}} p^{\mathrm{eq}}}{C_{\mathrm{Zn}_i^{+}}^{\mathrm{eq}}}, \tag{12}$$

where C_X^{eq} denotes the thermal equilibrium concentrations of the particular point defect for the underlying doping conditions. Assuming that the hole concentration p is mainly determined by the concentration of the acceptor, the neutrality equation yields

$$p = \tfrac{1}{2} (C_{\mathrm{Zn}_{\mathrm{Ga}}^{-}} + \sqrt{(C_{\mathrm{Zn}_{\mathrm{Ga}}^{-}})^2 + 4n_i^2}) \tag{13}$$

and

$$p^{\mathrm{eq}} = \tfrac{1}{2} (C_{\mathrm{Zn}_{\mathrm{Ga}}^{-}}^{\mathrm{eq}} + \sqrt{(C_{\mathrm{Zn}_{\mathrm{Ga}}^{-}}^{\mathrm{eq}})^2 + 4n_i^2}). \tag{14}$$

n_i is the intrinsic carrier concentration in GaAs.[22] With Eq. (13) the term $(1/p)(\partial p/\partial x)$ in Eqs. (8) and (10), which accounts for the effect of the electric field on the diffusion of charged defects,[12] is replaced with

$$\frac{1}{p} \frac{\partial p}{\partial x} = \frac{1}{\sqrt{\tilde{C}_{\mathrm{Zn}_{\mathrm{Ga}}^{-}}^2 + 4\tilde{n}_i^2}} \frac{\partial \tilde{C}_{\mathrm{Zn}_{\mathrm{Ga}}^{-}}}{\partial x}, \tag{15}$$

where $\tilde{n}_i = n_i / p^{\mathrm{eq}}$ and $p^{\mathrm{eq}} \approx C_{\mathrm{Zn}_{\mathrm{Ga}}^{-}}^{\mathrm{eq}}$.

Numerical solutions of Eqs. (7)–(10) were calculated using a software package provided by Jüngling *et al.*,[19] which we have modified for our simulations. For the calculations the initial concentrations of the point defects were normalized to the respective thermal equilibrium concentrations after diffusion. The following values were assumed:

$$\tilde{C}_{\mathrm{Zn}_{\mathrm{Ga}}^{-}}(x, t=0) = \tilde{C}_{\mathrm{Zn}_i^{+}}(x, t=0) = 10^{-8}, \tag{16}$$

$$\tilde{C}_{I_{\mathrm{Ga}}^{0}}(x, t=0) = 1.0, \tag{17}$$

$$\tilde{C}_{I_{\mathrm{Ga}}^{+}}(x, t=0) = \tilde{n}_i. \tag{18}$$

Equation (16) takes into account that the concentration of $\mathrm{Zn}_{\mathrm{Ga}}$ and Zn_i prior to diffusion is below the detection limit of SIMS. The initial concentrations of I_{Ga}^{0} and I_{Ga}^{+} given by Eqs. (17) and (18) were considered to equal the thermal equilibrium concentrations under electronically intrinsic conditions. The thermal equilibrium concentration of I_{Ga}^{0} is independent of doping. Hence we obtain Eq. (17). The relationship

$$C_{I_{\mathrm{Ga}}^{+}}^{\mathrm{eq}}(p^{\mathrm{eq}}) = C_{I_{\mathrm{Ga}}^{+}}^{\mathrm{eq}}(n_i) \frac{p^{\mathrm{eq}}}{n_i} = \frac{C_{I_{\mathrm{Ga}}^{+}}^{\mathrm{eq}}(n_i)}{\tilde{n}_i} \tag{19}$$

describes the impact of doping on the formation of I_{Ga}^{+} (Ref. 20) and yields Eq. (18).

The boundary concentrations at $x=0$ were set to the thermal equilibrium concentrations under extrinsic conditions, i.e.,

TABLE I. Data of the model parameters $D^{\mathrm{eff}}_{\mathrm{Zn}^-_{\mathrm{Ga}}}$, $D^{*}_{I^0_{\mathrm{Ga}}}$, and $D^{*}_{I^+_{\mathrm{Ga}}}$ [see Eqs. (22)–(24)], which were determined from fitting the Zn profiles shown in Figs. 2 and 3. The diffusion parameters refer to extrinsic and Ga-rich conditions. $C^{\mathrm{eq}}_{\mathrm{Zn}^-_{\mathrm{Ga}}}$ equals the Zn surface concentration, which was considered for the simulations.

T (°C)	t (s)	$C^{\mathrm{eq}}_{\mathrm{Zn}^-_{\mathrm{Ga}}}$ (cm^{-3})	$D^{\mathrm{eff}}_{\mathrm{Zn}^-_{\mathrm{Ga}}}$ ($\mathrm{cm}^2\,\mathrm{s}^{-1}$)	$D^{*}_{I^0_{\mathrm{Ga}}}$ ($\mathrm{cm}^2\,\mathrm{s}^{-1}$)	$D^{*}_{I^+_{\mathrm{Ga}}}$ ($\mathrm{cm}^2\,\mathrm{s}^{-1}$)
620	10800	4.0×10^{18}	1.4×10^{-13}	1.4×10^{-18}	8.4×10^{-17}
671	3600	5.0×10^{18}	2.1×10^{-13}	9.1×10^{-18}	3.3×10^{-17}
671	7200	4.0×10^{18}	2.5×10^{-13}	1.3×10^{-17}	2.5×10^{-16}
720	3600	5.0×10^{18}	4.9×10^{-13}	2.7×10^{-16}	2.4×10^{-15}
770	3600	6.0×10^{18}	2.6×10^{-12}	3.2×10^{-15}	6.7×10^{-15}
820	1800	7.5×10^{18}	5.5×10^{-12}	8.4×10^{-15}	1.1×10^{-13}
820	3600	6.0×10^{18}	6.8×10^{-12}	5.2×10^{-14}	8.6×10^{-14}
870	1800	1.8×10^{19}	3.3×10^{-11}	5.3×10^{-14}	5.1×10^{-13}
870	1800	1.0×10^{19}	1.7×10^{-11}	1.6×10^{-13}	3.3×10^{-13}

$$\widetilde{C}_{\mathrm{Zn}^-_{\mathrm{Ga}}}(x=0,t)=\widetilde{C}_{\mathrm{Zn}^+_i}(x=0,t)=1.0,$$

$$\widetilde{C}_{I^0_{\mathrm{Ga}}}(x=0,t)=\widetilde{C}_{I^+_{\mathrm{Ga}}}(x=0,t)=1.0. \tag{20}$$

At the boundary $x=d$ we chose the conditions

$$\left.\frac{\partial\widetilde{C}_{\mathrm{Zn}^-_{\mathrm{Ga}}}}{\partial x}\right|_{x=d}=\left.\frac{\partial\widetilde{C}_{\mathrm{Zn}^+_i}}{\partial x}\right|_{x=d}=0,$$

$$\left.\frac{\partial\widetilde{C}_{I^0_{\mathrm{Ga}}}}{\partial x}\right|_{x=d}=\left.\frac{\partial\widetilde{C}_{I^+_{\mathrm{Ga}}}}{\partial x}\right|_{x=d}=0. \tag{21}$$

B. Fitting of Zn profiles

The Zn profiles shown in Figs. 2 and 3 were modeled by solving Eqs. (7)–(10) numerically under the initial and boundary conditions given by Eqs. (16)–(21). For the simulations we used $C^{\mathrm{eq}}_{\mathrm{Zn}^+_i}/C^{\mathrm{eq}}_{\mathrm{Zn}^-_{\mathrm{Ga}}}=10^{-4}$, $C^{\mathrm{eq}}_{I^0_{\mathrm{Ga}}}/C^{\mathrm{eq}}_{\mathrm{Zn}^-_{\mathrm{Ga}}}=10^{-8}$, $C^{\mathrm{eq}}_{I^+_{\mathrm{Ga}}}/C^{\mathrm{eq}}_{\mathrm{Zn}^-_{\mathrm{Ga}}}=10^{-8}$, $k_b' C^{\mathrm{eq}}_{I^0_{\mathrm{Ga}}}(p^{\mathrm{eq}})^2=1.0\ \mathrm{s}^{-1}$, and $k_b'' C^{\mathrm{eq}}_{I^+_{\mathrm{Ga}}} p^{\mathrm{eq}}=1.0\ \mathrm{s}^{-1}$. Other values for these model parameters do not significantly affect the calculated profiles. This holds as long as the factors $k_b' C^{\mathrm{eq}}_{I^0_{\mathrm{Ga}}}(p^{\mathrm{eq}})^2$ and $k_b'' C^{\mathrm{eq}}_{I^+_{\mathrm{Ga}}} p^{\mathrm{eq}}$ ensure local equilibrium of the kick-out reaction for times that are small compared to the total diffusion time. In the case when local equilibrium is established, Zn diffusion is fairly insensitive to the equilibrium concentrations C^{eq}_X ($X=\mathrm{Zn}_i, I_{\mathrm{Ga}}$). Then the profiles are mainly determined by the three parameters

$$D^{\mathrm{eff}}_{\mathrm{Zn}^-_{\mathrm{Ga}}}=C^{\mathrm{eq}}_{\mathrm{Zn}^+_i}D_{\mathrm{Zn}^+_i}/C^{\mathrm{eq}}_{\mathrm{Zn}^-_{\mathrm{Ga}}}, \tag{22}$$

$$D^{*}_{I^0_{\mathrm{Ga}}}=C^{\mathrm{eq}}_{I^0_{\mathrm{Ga}}}D_{I^0_{\mathrm{Ga}}}/C^{\mathrm{eq}}_{\mathrm{Zn}^-_{\mathrm{Ga}}}, \tag{23}$$

$$D^{*}_{I^+_{\mathrm{Ga}}}=C^{\mathrm{eq}}_{I^+_{\mathrm{Ga}}}D_{I^+_{\mathrm{Ga}}}/C^{\mathrm{eq}}_{\mathrm{Zn}^-_{\mathrm{Ga}}}. \tag{24}$$

Solid lines in Figs. 2 and 3 represent best fits to the experimental profiles. For fitting the solver for coupled partial differential equations was combined with the PROFILE optimization driver.[21] The values determined for the model parameters (22)–(24) are summarized in Table I together with the equilibrium Zn dopant concentration $C^{\mathrm{eq}}_{\mathrm{Zn}^-_{\mathrm{Ga}}}$ established at the surface. All diffusion coefficients listed in Table I refer to Ga-rich and extrinsic doping conditions.

C. Fitting of earlier Zn and Cd profiles

Figures 6 and 7 illustrate acceptor dopant profiles of Zn and Cd from the literature. The solid lines are best fits, which were obtained on the basis of reactions (2)–(4).[17] Fitting provides data for the model parameters $D^{\mathrm{eff}}_{\mathrm{Zn}^-_{\mathrm{Ga}}}$ and $D^{*}_{I^0_{\mathrm{Ga}}}$, which are compared in Sec. IV with the results from the S-shaped Zn profiles.

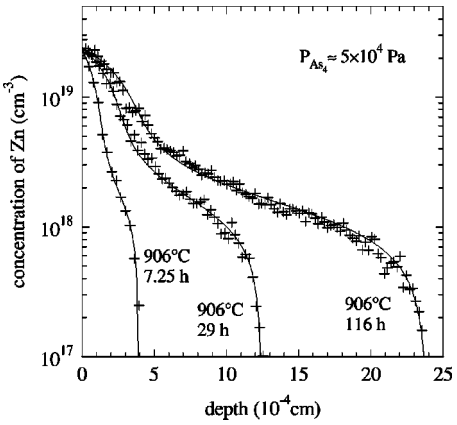

FIG. 6. Evolution of Zn concentration profiles in GaAs measured by Bösker *et al.* (Ref. 13) using spreading-resistance profiling after Zn diffusion at 906 °C under an As_4 pressure of $P_{As_4}=5\times10^4$ Pa for times as indicated. These authors originally described their profiles on the basis of the kick-out mechanism (5) with I^{2+}_{Ga} and I^{3+}_{Ga}. Our analysis on the basis of reactions (2)–(4) not only provided an accurate fit (see solid lines) but also solved the self-compensation problem associated with the $I^{2+,3+}_{\mathrm{Ga}}$-controlled mode of Zn diffusion.

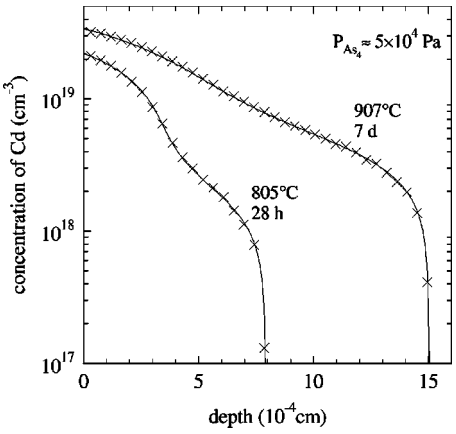

FIG. 7. Concentration profiles of Cd in GaAs measured by Bösker *et al.* (Ref. 16) with SIMS after diffusion under an As_4 pressure of $P_{As_4}=5\times10^4$ Pa at temperatures and times as indicated. These authors originally described their profiles on the basis of the kick-out mechanism (5) with I_{Ga}^{2+} and I_{Ga}^{3+}.[16] Solid lines represent our best fits to their data obtained on the basis of reactions (2)–(4).

IV. RESULTS

A. Zn-related diffusion coefficient

In order to compare the Zn-related diffusion coefficient $D^{\text{eff}}_{Zn^-_{Ga}}$ with data given in the literature, $D^{\text{eff}}_{Zn^-_{Ga}}$ was reduced to an As vapor pressure of $P_{As_4}=10^5$ Pa and electronically intrinsic conditions ($p=n=n_i$). This transformation to standard conditions is described by[12]

$$D^{\text{eff}}_{Zn^-_{Ga},r} = D^{\text{eff}}_{Zn^-_{Ga}}\left(\frac{n_i}{p^{\text{eq}}}\right)^2\left(\frac{P_{As_4}}{10^5\ \text{Pa}}\right). \quad (25)$$

P_{As_4} represents the partial pressure of As for Ga-rich conditions. We used the data reported by Arthur[23] for P_{As_4}, which are approximated by

$$P_{As_4}(\text{Ga}-\text{rich}) = 8.1\times10^{21}\exp\left(-\frac{5.44\ \text{eV}}{k_BT}\right)\ \text{Pa}. \quad (26)$$

$D^{\text{eff}}_{Zn^-_{Ga},r}$ was calculated with Eq. (25) taking into account $p^{\text{eq}} \approx C^{\text{eq}}_{Zn^-_{Ga}}$ (see Table I) and the data of n_i given by Blakemore[22] (see Table II). The results are listed in Table II and illustrated in Fig. 8 as solid symbols. The plus symbols represent data that we obtained from the analysis of kink-and-tail profiles given in the literature[13,24] (see Fig. 6). The open circles are data that were deduced from modeling the simultaneous diffusion of Zn and Ga in GaAs isotope multilayer structures.[17]. Figure 8 demonstrates that all $D^{\text{eff}}_{Zn^-_{Ga},r}$ data are consistent. The temperature dependence is best described by

$$D^{\text{eff}}_{Zn^-_{Ga},r} = (2.9^{+4.5}_{-1.8})10^2\exp\left(-\frac{(4.24\pm0.08)\ \text{eV}}{k_BT}\right)\frac{\text{cm}^2}{\text{s}} \quad (27)$$

and illustrated by the solid line in Fig. 8. The dashed line represents the result reported by Yu *et al.*,[12] who have analyzed Zn diffusion under isoconcentration conditions.[25,26] Without extensive modeling isoconcentration diffusion studies provide direct measures of $D^{\text{eff}}_{Zn^-_{Ga}}$ for the underlying background doping concentration. The good agreement between the data of $D^{\text{eff}}_{Zn^-_{Ga},r}$ reported in this work and the results of the isoconcentration diffusion experiments support our analysis of Zn diffusion in GaAs.

B. I^0_{Ga}- and I^+_{Ga}-related diffusion coefficients

Data for $D^*_{I^0_{Ga}}$ and $D^*_{I^+_{Ga}}$ obtained from fitting the Zn profiles shown in Figs. 2 and 3 are listed in Table I. In addition, kink-and-tail Zn and Cd profiles illustrated in Figs. 6 and 7 also yield data of $D^*_{I^0_{Ga}}$. According to Eq. (23), $D^*_{I^0_{Ga}}$ is corre-

TABLE II. The reduced Zn-related effective diffusion coefficient $D^{\text{eff}}_{Zn^-_{Ga},r}$ and the individual contributions $D^{I^0_{Ga}}_{Ga}$ and $D^{I^+_{Ga}}_{Ga}$ of neutral and positively charged Ga interstitials I^0_{Ga} and I^+_{Ga} to Ga diffusion in GaAs. All data refer to standard conditions, i.e., to electronically intrinsic conditions and an As pressure of 10^5 Pa. The data were derived from Eqs. (25), (31), and (32) taking into account the results listed in Table I. For the intrinsic carrier concentration n_i we used the values reported by Blakemore.[22] The As_4 pressure (P_{As_4}) for Ga-rich conditions was calculated with Eq. (26).

T (°C)	n_i (cm^{-3})	$(P_{As_4})^{1/4}$ (Pa$^{1/4}$)	$D^{\text{eff}}_{Zn^-_{Ga},r}$ (cm^2 s^{-1})	$D^{I^0_{Ga}}_{Ga}$ (cm^2 s^{-1})	$D^{I^+_{Ga}}_{Ga}$ (cm^2 s^{-1})
620	9.1×10^{15}	6.3×10^{-3}	2.7×10^{-22}	9.0×10^{-26}	1.2×10^{-26}
671	1.8×10^{16}	1.6×10^{-2}	2.6×10^{-21}	1.9×10^{-24}	2.5×10^{-26}
671	1.8×10^{16}	1.6×10^{-2}	4.7×10^{-21}	2.2×10^{-24}	1.9×10^{-25}
720	3.4×10^{16}	3.7×10^{-2}	4.7×10^{-20}	1.3×10^{-22}	7.6×10^{-24}
770	6.0×10^{16}	8.0×10^{-2}	1.2×10^{-18}	3.9×10^{-21}	8.1×10^{-23}
820	1.0×10^{17}	1.6×10^{-1}	9.2×10^{-18}	2.5×10^{-20}	4.7×10^{-21}
820	1.0×10^{17}	1.6×10^{-1}	9.2×10^{-18}	2.5×10^{-20}	4.7×10^{-21}
820	1.0×10^{17}	1.6×10^{-1}	1.8×10^{-17}	1.3×10^{-19}	3.6×10^{-21}
870	1.7×10^{17}	3.0×10^{-1}	5.1×10^{-17}	7.1×10^{-19}	6.5×10^{-20}
870	1.7×10^{17}	3.0×10^{-1}	7.9×10^{-17}	1.2×10^{-18}	4.2×10^{-20}

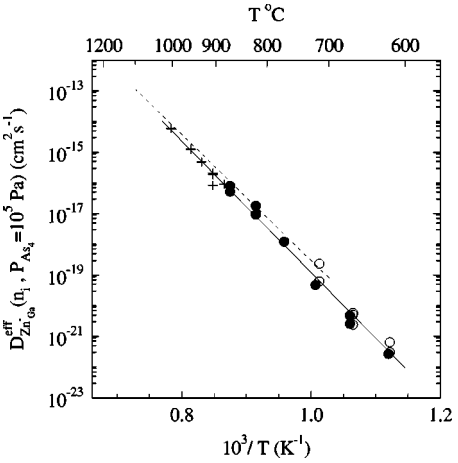

FIG. 8. Temperature dependence of the reduced Zn diffusivity $D^{\mathrm{eff}}_{\mathrm{Zn}^-_{\mathrm{Ga}},r}$ determined from Zn diffusion in GaAs under Ga-rich conditions [●: this work; ○: (Ref. 17)] and from Zn diffusion under an As_4 pressure of $P_{\mathrm{As}_4}\approx 5\times 10^4$ Pa [+: our analysis of Zn profiles measured by Bösker *et al.* (Refs. 13 and 24)]. The solid line represents the best fit to all $D^{\mathrm{eff}}_{\mathrm{Zn}^-_{\mathrm{Ga}},r}$ data, which is reproduced by Eq. (27). The dashed line shows the temperature dependence deduced by Yu *et al.* (Ref. 12) from Zn diffusion experiments under isoconcentration conditions performed by Casey *et al.*[25,26] [$D^{\mathrm{eff}}_{\mathrm{Zn}^-_{\mathrm{Ga}},r}=96.8\exp(-4.07\ \mathrm{eV}/k_BT)\ \mathrm{cm}^2\,\mathrm{s}^{-1}$].

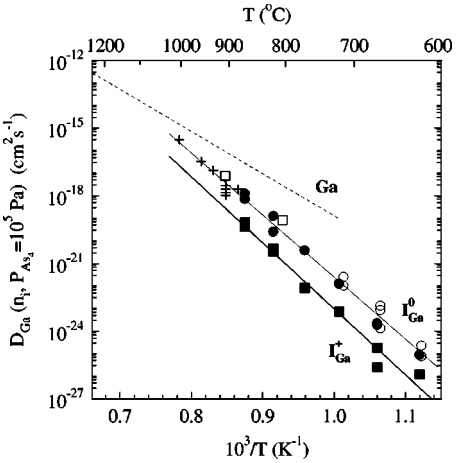

FIG. 9. Temperature dependence of the individual contributions of I^0_{Ga} [●: this work; ○: (Ref. 17); +: our analysis of Zn profiles measured by Bösker *et al.* (Refs. 13 and 24); □: our analysis of Cd profiles measured by Bösker *et al.* (Ref. 16)] and of I^+_{Ga} (■: this work) to Ga diffusion in GaAs in comparison to the directly measured Ga diffusion coefficient D_{Ga} in GaAs (dashed line) (Refs. [32,33]). The individual contributions and the Ga diffusivity were reduced to standard conditions, i.e., electronically intrinsic conditions and an As_4 pressure of 10^5 Pa. The temperature dependence of D_{Ga} is given by Eq. (30).

lated with the product $C^{\mathrm{eq}}_{I^0_{\mathrm{Ga}}} D_{I^0_{\mathrm{Ga}}}$. This product is associated with the Ga diffusion coefficient D_{Ga} in GaAs. D_{Ga} is given by the sum of the individual contributions of charged Ga interstitials I^k_{Ga} and charged Ga vacancies V^r_{Ga} to Ga diffusion, i.e.,

$$D_{\mathrm{Ga}} = \frac{1}{C_o}\left(\sum_{k=0}^{3+} f_k C^{\mathrm{eq}}_{I^k_{\mathrm{Ga}}} D_{I^k_{\mathrm{Ga}}} + \sum_{r=3-}^{1+} f_r C^{\mathrm{eq}}_{V^r_{\mathrm{Ga}}} D_{V^r_{\mathrm{Ga}}}\right) = \sum_{k=0}^{3+} D^{I^k_{\mathrm{Ga}}}_{\mathrm{Ga}} + \sum_{r=3-}^{1+} D^{V^r_{\mathrm{Ga}}}_{\mathrm{Ga}}. \quad (28)$$

Equation (28) assumes that Ga diffusion is restricted to the Ga sublattice, i.e., no interference between Ga and As diffusion is considered. $f_{k,r}$ denotes the diffusion correlation factor. For simplicity we assume $f_{k,r}\approx 1$ for both native defects and all possible charge states. The charge states considered in Eq. (28) are in accordance with the predictions of theoretical calculations.[27,28] In addition a contribution of I^0_{Ga} was assumed. The quantity

$$D^Y_{\mathrm{Ga}} = C^{\mathrm{eq}}_Y D_Y / C_o \quad (29)$$

denotes the individual contribution of the native point defect $Y=I^k_{\mathrm{Ga}}, V^r_{\mathrm{Ga}}$ to Ga diffusion in GaAs. C_o(=2.215 $\times 10^{22}$ cm^{-3}) is the Ga atom density in GaAs.

Ga diffusion in undoped and extrinsically doped GaAs has been extensively investigated by means of ^{69}GaAs/^{71}GaAs isotope heterostructures.[29–34] Based on the arguments given in Refs. 32–34, Ga diffusion under intrinsic conditions and $P_{\mathrm{As}_4}=10^5$ Pa is described by[33]

$$D_{\mathrm{Ga}} = (0.64^{+0.61}_{-0.31})\exp\left(-\frac{(3.71\pm 0.07)\ \mathrm{eV}}{k_BT}\right)\frac{\mathrm{cm}^2}{\mathrm{s}}. \quad (30)$$

This temperature dependence of Ga diffusion is shown in Fig. 9 by the dashed line.

In order to determine the contributions $D^{I^0_{\mathrm{Ga}}}_{\mathrm{Ga}}$ and $D^{I^+_{\mathrm{Ga}}}_{\mathrm{Ga}}$ to Ga diffusion, the model parameters $D^*_{I^0_{\mathrm{Ga}}}$ and $D^*_{I^+_{\mathrm{Ga}}}$, which are defined by Eqs. (23) and (24) and listed in Table I, were multiplied with $C^{\mathrm{eq}}_{\mathrm{Zn}^-_{\mathrm{Ga}}}/C_o$ and reduced to standard conditions ($p=n_i$ and $P_{\mathrm{As}_4}=10^5$ Pa) according to the relationships

$$D^{I^0_{\mathrm{Ga}}}_{\mathrm{Ga}}(n_i, 10^5\ \mathrm{Pa}) = D^*_{I^0_{\mathrm{Ga}}}\frac{C^{\mathrm{eq}}_{\mathrm{Zn}^-_{\mathrm{Ga}}}}{C_o}\left(\frac{P_{\mathrm{As}_4}}{10^5\ \mathrm{Pa}}\right)^{0.25}, \quad (31)$$

$$D^{I^+_{\mathrm{Ga}}}_{\mathrm{Ga}}(n_i, 10^5\ \mathrm{Pa}) = D^*_{I^+_{\mathrm{Ga}}}\frac{C^{\mathrm{eq}}_{\mathrm{Zn}^-_{\mathrm{Ga}}}}{C_o}\frac{n_i}{p^{\mathrm{eq}}}\left(\frac{P_{\mathrm{As}_4}}{10^5\ \mathrm{Pa}}\right)^{0.25}. \quad (32)$$

The last factor of Eqs. (31) and (32) accounts for the As_4 pressure dependence of $D^*_{I^{0,+}_{\mathrm{Ga}}}$ via $C^{\mathrm{eq}}_{I^{0,+}_{\mathrm{Ga}}}$ [see Eqs. (23) and (24)] and reduces $D^{I^{0,+}_{\mathrm{Ga}}}_{\mathrm{Ga}}$ to $P_{\mathrm{As}_4}=10^5$ Pa.[35] The factor n_i/p^{eq} in Eq. (32) reduces $D^*_{I^+_{\mathrm{Ga}}}$, which depends on the doping level via $C^{\mathrm{eq}}_{I^+_{\mathrm{Ga}}}(p^{\mathrm{eq}}, P_{\mathrm{As}_4})$ [see Eq. (19)], to intrinsic conditions. Taking into account the data of $C^{\mathrm{eq}}_{\mathrm{Zn}^-_{\mathrm{Ga}}}$, $D^*_{I^{0,+}_{\mathrm{Ga}}}$, n_i and $(P_{\mathrm{As}_4})^{0.25}$ given in Tables I and II, and the approximation $p^{\mathrm{eq}}\approx C^{\mathrm{eq}}_{\mathrm{Zn}^-_{\mathrm{Ga}}}$, $D^{I^0_{\mathrm{Ga}}}_{\mathrm{Ga}}$ and $D^{I^+_{\mathrm{Ga}}}_{\mathrm{Ga}}$ were calculated with Eqs. (31) and (32). The results are listed in Table II.

The contributions $D_{\mathrm{Ga}}^{I_{\mathrm{Ga}}^0}$ and $D_{\mathrm{Ga}}^{I_{\mathrm{Ga}}^+}$ to Ga diffusion are shown in Fig. 9 in comparison to D_{Ga}. The solid symbols represent $D_{\mathrm{Ga}}^{I_{\mathrm{Ga}}^{0,+}}$ data that were deduced from the S-shaped Zn profiles of Figs. 2 and 3. The plus signs and open boxes are results for $D_{\mathrm{Ga}}^{I_{\mathrm{Ga}}^0}$ from Zn and Cd profiles given in the literature, respectively (see, e.g., Figs. 6 and 7). The open circles show $D_{\mathrm{Ga}}^{I_{\mathrm{Ga}}^0}$ data that were obtained from the analysis of Zn diffusion in GaAs isotope multilayer structures.[17] Figure 9 clearly demonstrates that all results for $D_{\mathrm{Ga}}^{I_{\mathrm{Ga}}^0}$ are consistent. The temperature dependence of $D_{\mathrm{Ga}}^{I_{\mathrm{Ga}}^0}$ is described by

$$D_{\mathrm{Ga}}^{I_{\mathrm{Ga}}^0} = (7.5^{+20.7}_{-5.5})10^5 \exp\left(-\frac{(5.45 \pm 0.12)\ \mathrm{eV}}{k_B T}\right) \frac{\mathrm{cm}^2}{\mathrm{s}}. \tag{33}$$

The temperature dependence of $D_{\mathrm{Ga}}^{I_{\mathrm{Ga}}^+}$ is illustrated by the lower solid line in Fig. 9 and reproduced by

$$D_{\mathrm{Ga}}^{I_{\mathrm{Ga}}^+} = (1.8^{+690}_{-1.7})10^6 \exp\left(-\frac{(5.80 \pm 0.32)\ \mathrm{eV}}{k_B T}\right) \frac{\mathrm{cm}^2}{\mathrm{s}}. \tag{34}$$

Equations (33) and (34) represent the individual contributions of I_{Ga}^0 and I_{Ga}^+ to Ga diffusion in GaAs for a wide temperature range.

V. DISCUSSION

The experimental realization of S-shaped Zn diffusion profiles that develop with decreasing Zn surface concentration (see Fig. 1) was essential for the finding that I_{Ga}^0 and I_{Ga}^+ are involved in the diffusion of Zn in GaAs. The kick-out model with neutral and singly positively charged Ga interstitials predicts S-shaped Zn profiles, which yield an accurate description of the experimental Zn profiles as illustrated by the solid lines in Figs. 2 and 3. Fitting provides results for the individual contributions of I_{Ga}^0 and I_{Ga}^+ to Ga diffusion, which, after reduction to standard conditions, are lower than the directly measured Ga self-diffusion coefficient (see Fig. 9). This is consistent with the general understanding that Ga diffusion in GaAs under standard conditions is mainly controlled by Ga vacancies (see, e.g., Ref. 34 and references therein). For Zn surface concentrations exceeding 10^{19} cm^{-3} the convex shape of the Zn profile near the surface is covered by a concave profile. These often observed kink-and-tail acceptor dopant profiles are accurately described on the basis of reactions (2)–(4) (see Ref. 17 and Figs. 6 and 7). The analysis of kink-and-tail profiles, which according to transmission electron microscopy analyses of the samples are not associated with the formation of microscopic defects,[13,16,24] provide data for the I_{Ga}^0 contribution to Ga diffusion that are in excellent agreement with the results obtained from the analysis of the S-shaped Zn profiles. This shows that the tail part of Zn profiles both in the case of S-shaped and kink-and-tail profiles is mainly mediated by I_{Ga}^0.

So far, kink-and-tail profiles treated in the literature were mainly described on the basis of an I_{Ga}^{2+}- and I_{Ga}^{3+}-controlled kick-out diffusion mechanism.[13,16] Although this model provides a fairly good fit to the experimental profiles, it suffers from an inconsistency related to the electrical compensation of $\mathrm{Zn}_{\mathrm{Ga}}^-$ by I_{Ga}^{2+}.[13,36] This inconsistency is resolved when neutral Ga interstitials mediate Zn diffusion. The accurate fits to the experimental Zn and Cd profiles shown in this work, the overall consistency of the $I_{\mathrm{Ga}}^{0,+}$-related diffusion data with the Ga self-diffusion coefficient in GaAs, and finally the clarification of the compensation problem associated with the former Zn diffusion model strongly support that $I_{\mathrm{Ga}}^{0,+}$ mediate acceptor dopant diffusion in GaAs rather than $I_{\mathrm{Ga}}^{2+,3+}$.

The temperature dependence of the I_{Ga}^0- and I_{Ga}^+ contributions to Ga diffusion is characterized with

$$D_{\mathrm{Ga}}^{I_{\mathrm{Ga}}^{0,+}} = D_0^{I_{\mathrm{Ga}}^{0,+}} \exp\left(-\frac{H_{I_{\mathrm{Ga}}^{0,+}}^{\mathrm{SD}}}{k_B T}\right), \tag{35}$$

where $H_{I_{\mathrm{Ga}}^{0,+}}^{\mathrm{SD}} (= H_{I_{\mathrm{Ga}}^{0,+}}^{f} + H_{I_{\mathrm{Ga}}^{0,+}}^{m})$ is the activation enthalpy for $I_{\mathrm{Ga}}^{0,+}$-mediated Ga diffusion in GaAs, which equals the sum of the formation enthalpy $H_{I_{\mathrm{Ga}}^{0,+}}^{f}$ and migration enthalpy $H_{I_{\mathrm{Ga}}^{0,+}}^{m}$ of the particular point defect. Comparison of Eq. (35) with Eqs. (33) and (34) yields $H_{I_{\mathrm{Ga}}^0}^{\mathrm{SD}} = 5.45$ eV and $H_{I_{\mathrm{Ga}}^+}^{\mathrm{SD}} = 5.80$ eV. The preexponential factor $D_0^{I_{\mathrm{Ga}}^{0,+}}$ is associated through

$$D_0^{I_{\mathrm{Ga}}^{0,+}} = g_{I_{\mathrm{Ga}}^{0,+}} a_0^2 \nu_0 \exp\left(\frac{S_{I_{\mathrm{Ga}}^{0,+}}^{\mathrm{SD}}}{k_B}\right) \tag{36}$$

with the corresponding activation entropy $S_{I_{\mathrm{Ga}}^{0,+}}^{\mathrm{SD}} (= S_{I_{\mathrm{Ga}}^{0,+}}^{f} + S_{I_{\mathrm{Ga}}^{0,+}}^{m})$, which equals the sum of the entropy of formation $S_{I_{\mathrm{Ga}}^{0,+}}^{f}$ and migration $S_{I_{\mathrm{Ga}}^{0,+}}^{m}$. $g_{I_{\mathrm{Ga}}^{0,+}}$ is a geometry factor that depends on the crystal structure and microscopic jump geometry. The factor a_0 is the lattice constant (5.65×10^{-10} m) and ν_0 is the attempt frequency. Assuming $g_{I_{\mathrm{Ga}}^{0,+}} \sim 1$ and an attempt frequency of the order of the Debye frequency ($\sim 10^{13}$ s^{-1}), the preexponential factors of Eqs. (33) and (34) yield $S_{I_{\mathrm{Ga}}^0}^{\mathrm{SD}} \approx 17 k_B$ and $S_{I_{\mathrm{Ga}}^+}^{\mathrm{SD}} \approx 18 k_B$. For comparison the preexponential factor $D_0 = 0.64$ cm^2 s^{-1} of Ga diffusion in GaAs [see Eq. (30)] yields a significantly lower activation entropy of $3k_B$. This value is attributed to the Ga vacancy. The high $S_{I_{\mathrm{Ga}}}^{\mathrm{SD}}$ indicates that the Ga interstitial in GaAs is spread out over several neighboring lattice sites, whereas the low $S_{V_{\mathrm{Ga}}}^{\mathrm{SD}}$ shows that the Ga vacancy is more localized. Similar native point defect properties were found for the self-interstitial and vacancy in silicon. The activation entropy for the vacancy-mediated Si self-diffusion yields $S_{V_{\mathrm{Si}}}^{\mathrm{SD}} = 5.5 k_B$. On the other hand an activation entropy of $S_{I_{\mathrm{Si}}}^{\mathrm{SD}} = 13.2 k_B$ was determined for the self-interstitial mediated Si self-diffusion.[37] This agreement between the activation entropies of native point defects in compound and elemental semiconductors suggests that the self-interstitial is always a more spread-out defect than the vacancy. An additional comparison of the activation enthalpy and entropy for I_{Ga}-mediated Ga diffusion in GaAs with theoretical results would be very helpful but to our knowledge no results were reported in the literature so far.

Finally, it is noted that modeling of kink-and-tail acceptor dopant profiles on the basis of reactions (2)–(4) also provides data for the individual contributions of V_{Ga}^{0} and V_{Ga}^{+} to Ga diffusion. The $V_{Ga}^{0,+}$ contributions obtained from Zn and Cd profiles for As-rich conditions exceed the contributions of $I_{Ga}^{0,+}$ and are in good agreement with Ga diffusion.[17] This is consistent with the general understanding that Ga diffusion in GaAs under standard conditions is mainly mediated by Ga vacancies. However, it was shown in Ref. 17 that kink-and-tail Zn profiles for Ga-rich conditions yield data for the V_{Ga} contribution that significantly exceed Ga diffusion. This inconsistency shows that the mechanism of Zn diffusion in GaAs under Ga-rich conditions is still not fully understood. But note, this only refers to the interpretation of the kink part of the kink-and-tail profiles observed under Ga-rich conditions. The tail of Zn and Cd profiles obtained after annealing under both Ga-rich and As-rich conditions provides $D_{Ga}^{I_{Ga}^{0}}$ data that are consistent (see Fig. 9).

VI. CONCLUSIONS

We have performed experiments on Zn diffusion in GaAs with a dilute Ga-Zn source. The obtained S-shaped diffusion profiles are accurately described on the basis of the kick-out mechanism taking into account neutral and singly positively charged Ga interstitials, i.e., I_{Ga}^{0} and I_{Ga}^{+}. Further evidence for $I_{Ga}^{0,+}$-mediated Zn diffusion is given by the successful modeling of kink-and-tail Zn and Cd profiles given in the literature and the fact that all data obtained for the I_{Ga}^{0} contribution to Ga diffusion are in excellent agreement (see Fig. 9). The I_{Ga}^{0} and I_{Ga}^{+} contributions to Ga diffusion are smaller than the total Ga diffusion coefficient. This is consistent with the general understanding that Ga diffusion in GaAs under standard conditions ($p=n_i$ and $P_{As_4}=10^5$ Pa) is mainly mediated by Ga vacancies. The temperature dependence of the $I_{Ga}^{0}(I_{Ga}^{+})$-mediated Ga diffusion is characterized by an activation enthalpy of (5.45 ± 0.12) eV [(5.80 ± 0.32) eV] and large preexponential factors [see Eqs. (33) and (34)]. These factors yield large activation entropies of $17k_B$ and $18k_B$ for I_{Ga}^{0}- and I_{Ga}^{+}-mediated Ga diffusion, respectively, and suggest that the Ga interstitial extends over several atomic volumes.

Our interpretation of $I_{Ga}^{0,+}$-mediated acceptor dopant diffusion in GaAs solves the inconsistency related to the compensation of the acceptor by I_{Ga}^{2+}. This doubly and, in addition, triply positively charged Ga interstitials were generally considered to control Zn diffusion in GaAs. The diffusion experiments presented in this work and our reanalysis of Zn and Cd diffusion profiles given in the literature disproves the earlier proposed diffusion model.

The present work reveals that acceptor dopant diffusion is affected by Ga interstitials both under Ga- and As-rich conditions. Under As-rich conditions an additional contribution of Ga vacancies is very likely and the good agreement between the contribution of Ga vacancies to Ga diffusion with the Ga diffusion coefficient supports this assumption.[17] However, one question still remains. This concerns the origin of the kink part of the kink-and-tail acceptor profiles that are observed under Ga-rich conditions and high doping levels ($>10^{19}$ cm^{-3}). This will be the subject of further investigations.

ACKNOWLEDGMENT

The authors thank N.A. Stolwijk for valuable discussions.

*Email address: bracht@uni-muenster.de

[1] H. R. Winteler, Helv. Phys. Acta **43**, 496 (1970); **44**, 451 (1971).
[2] C. H. Ting and G. L. Pearson, J. Appl. Phys. **42**, 2247 (1971).
[3] J. Blanc, J. Appl. Phys. **45**, 1948 (1974).
[4] B. Tuck and A. J. N. Houghton, J. Phys. D **14**, 2147 (1981).
[5] U. Gösele and F. Morehead, J. Appl. Phys. **52**, 4617 (1981).
[6] O. Hildebrand, Phys. Status Solidi A **72**, 575 (1982).
[7] A. H. van Ommen, J. Appl. Phys. **54**, 5055 (1983).
[8] D. Shaw, Phys. Status Solidi A **86**, 629 (1984).
[9] B. Tuck, J. Phys. D **18**, 557 (1985).
[10] D. G. Deppe and N. Holonyak, Jr., J. Appl. Phys. **64**, R93 (1988).
[11] R. M. Cohen, J. Appl. Phys. **67**, 7288 (1990).
[12] S. Yu, T. Y. Tan, and U. Gösele, J. Appl. Phys. **69**, 3547 (1991).
[13] G. Bösker, N. A. Stolwijk, H.-G. Hettwer, A. Rucki, W. Jäger, and U. Södervall, Phys. Rev. B **52**, 11 927 (1995).
[14] M. Luysberg, W. Jäger, K. Urban, M. Schänzer, N. A. Stolwijk, and H. Mehrer, Mater. Sci. Eng., B **13**, 137 (1992).
[15] W. Jäger, A. Rucki, K. Urban, H.-G. Hettwer, N. A. Stolwijk, H. Mehrer, and T. Y. Tan, J. Appl. Phys. **74**, 4409 (1993).
[16] G. Bösker, N. A. Stolwijk, H. Mehrer, U. Södervall, and W. Jäger, J. Appl. Phys. **86**, 791 (1999).
[17] H. Bracht, M. S. Norseng, E. E. Haller, and K. Eberl, Physica B **308–310**, 831 (2001).
[18] W. D. Laidig, N. Holonyak, Jr., M. D. Camras, K. Hess, J. J. Coleman, P. D. Dapkus, and J. Bardeen, Appl. Phys. Lett. **38**, 776 (1981).
[19] W. Jüngling, P. Pichler, S. Selberherr, E. Guerrero, and H. W. Pötzl, IEEE Trans. Electron Devices **ED-32**, 156 (1985).
[20] W. Shockley and J. L. Moll, Phys. Rev. **119**, 1480 (1960).
[21] G. L. J. Ouwerling, Doctoral thesis, Delft University of Technology, 1989.
[22] J. S. Blakemore, J. Appl. Phys. **53**, R123 (1982).
[23] J. R. Arthur, J. Phys. Chem. Solids **28**, 2257 (1967).
[24] G. Bösker, Doctoral thesis, University of Münster, 1999.
[25] H. C. Casey, M. B. Panish, and L. L. Chang, Phys. Rev. **162**, 660 (1967).
[26] H. C. Casey and M. B. Panish, Trans. Metall. Soc. AIME **242**, 406 (1968).
[27] G. A. Baraff and M. Schlüter, Phys. Rev. Lett. **55**, 1327 (1985).
[28] M. Bockstedte, Doctoral thesis, University of Erlangen-Nürnberg, 1999.
[29] T. Y. Tan, H. M. You, S. Yu, U. M. Gösele, W. Jäger, D. W. Boeringer, F. Zypman, R. Tsu, and S.-T. Lee, J. Appl. Phys. **72**, 5206 (1992).
[30] L. Wang, L. Hsu, E. E. Haller, J. W. Erickson, A. Fischer, K. Eberl, and M. Cardona, Phys. Rev. Lett. **76**, 2342 (1996).

[31] K. Muraki and Y. Horikoshi, Inst. Phys. Conf. Ser. **145**, 547 (1996).
[32] H. Bracht, E. E. Haller, K. Eberl, M. Cardona, and R. Clark-Phelps, Mater. Res. Soc. Symp. Proc. **527**, 335 (1998).
[33] H. Bracht, E. E. Haller, K. Eberl, and M. Cardona, Appl. Phys. Lett. **74**, 49 (1999).
[34] H. Bracht, M. Norseng, E. E. Haller, K. Eberl, and M. Cardona, Solid State Commun. **112**, 301 (1999).
[35] T. Y. Tan, Mater. Sci. Eng., B **10**, 227 (1991).
[36] N. A. Stolwijk and J. Pöpping, Mater. Sci. Semicond. Process. **6**, 315 (2003).
[37] H. Bracht, N. A. Stolwijk, and H. Mehrer, Phys. Rev. B **52**, 16 542 (1995).